

Two waves of massive stars running away from the young cluster R136

<https://doi.org/10.1038/s41586-024-08013-8>

Received: 1 May 2024

Accepted: 4 September 2024

Published online: 09 October 2024

 Check for updates

Mitchel Stoop¹✉, Alex de Koter^{1,2}, Lex Kaper¹, Sarah Brands¹, Simon Portegies Zwart³, Hugues Sana², Fiorenzo Stoppa⁴, Mark Gieles^{5,6}, Laurent Mahy⁷, Tomer Shenar⁸, Difeng Guo¹, Gijs Nelemans^{2,4,9} & Steven Rieder^{2,10}

Massive stars are predominantly born in stellar associations or clusters¹. Their radiation fields, stellar winds and supernovae strongly impact their local environment. In the first few million years of a cluster's life, massive stars are dynamically ejected and run away from the cluster at high speed². However, the production rate of dynamically ejected runaways is poorly constrained. Here we report on a sample of 55 massive runaway stars ejected from the young cluster R136 in the Large Magellanic Cloud. An astrometric analysis of Gaia data^{3–5} reveals two channels of dynamically ejected runaways. The first channel ejects massive stars in all directions and is consistent with dynamical interactions during and after the birth of R136. The second channel launches stars in a preferred direction and may be related to a cluster interaction. We found that 23–33% of the most luminous stars initially born in R136 are runaways. Model predictions^{2,6,7} have significantly underestimated the dynamical escape fraction of massive stars. Consequently, their role in shaping and heating the interstellar and galactic media and their role in driving galactic outflows are far more important than previously thought^{8,9}.

The Large Magellanic Cloud (LMC), a satellite galaxy of the Milky Way, hosts the Tarantula nebula (30 Doradus), a region containing more than a thousand massive stars that formed in several bursts of star formation in the past several tens of megayears¹⁰. The most recent star-formation episode in this region gave birth to the dense cluster core Radcliffe 136 (R136). Using the astrometric information in Gaia Data Release 3 (DR3)^{3–5}, we identified stars consistent with running away from R136 (Methods). We required them to have a transverse velocity significantly larger than 27.6 km s⁻¹ and to have been ejected up to 3 Myr ago, although R136 is probably younger. This yielded 55 early-type runaways, which is an increase of the number of known runaways from the cluster core by an order of magnitude^{11–13}. We determined their dynamic trace-back age (kinematic age), which indicates how long ago they were ejected from R136, and cross-matched them with the literature to obtain their stellar parameters (Supplementary Information).

The spectral type of almost all the classified runaways ranges from early-type B to early-type O. There are also WN(h)-type stars. The corresponding masses are in the range of approximately 5 up to 140 M_⊙. The runaways are moving in different directions (Fig. 1) and have reached (projected) distances of approximately 3 to 460 pc from R136. This implies that about half of them have left the 30 Dor region and that their ionizing radiation fields, supersonic stellar winds and, eventually, powerful supernovae are affecting relatively tenuous areas in or outside the LMC.

Notably, we found that the runaways are not consistent with being ejected isotropically (Fig. 2). If they had, we would expect them to have been ejected in a random direction by dynamical interactions between

a binary and at least a single star⁶. More specifically, a subsample of 18 runaways with kinematic ages less than 1.0 Myr contains 16 runaways that were ejected to the north of R136. We rejected the hypothesis that the overabundance of runaways ejected in a northern direction (position angle 20–150 deg) was due to an isotropic ejection mechanism to 7×10^{-4} significance (Supplementary Information). This indicates that these recent runaways were ejected in a preferred direction, which was not observed for the runaways with a kinematic age of over 1.0 Myr.

The kinematic age distribution in Fig. 3 shows when the runaway stars were ejected. The intrinsic distribution of the kinematic ages was estimated using Gaussian kernel density estimation, which revealed peaks around 0.2 and 1.8 Myr, after which the distribution tails off. The runaway ejection efficiency is lowest around approximately 1.0 Myr. We conclude that the kinematic age distribution is not consistent with a constant ejection rate to 2.5σ significance. The peaks and dips in the observed kernel density estimation cannot be explained by stochastic sampling of the runaways. We interpreted the peaks around 0.2 and 1.8 Myr as separate ejection events, as few to no runaways were ejected about 1.0 Myr ago. The anisotropic nature of runaways with kinematic ages less than 1.0 Myr relative to the isotropic nature of the runaways with larger kinematic ages also points to two distinct ejection events.

The onset of a dynamical runaway ejection may occur during or shortly after the formation of a cluster^{2,14}, as observed in several Galactic young massive clusters^{15,16}. The age of R136 is 1–2.5 Myr (ref. 17). Therefore, we identified the peak in the kinematic age distribution approximately 1.8 Myr ago as the onset of the dynamical ejection of massive stars as part of the formation process of R136. Assuming that

¹Anton Pannekoek Institute for Astronomy, University of Amsterdam, Amsterdam, The Netherlands. ²Institute of Astronomy, KU Leuven, Leuven, Belgium. ³Leiden Observatory, Leiden University, Leiden, The Netherlands. ⁴Department of Astrophysics/IMAPP, Radboud University, Nijmegen, The Netherlands. ⁵ICREA, Barcelona, Spain. ⁶Institut de Ciències del Cosmos (ICCUB), Universitat de Barcelona (IEEC-UB), Barcelona, Spain. ⁷Royal Observatory of Belgium, Brussels, Belgium. ⁸The School of Physics and Astronomy, Tel Aviv University, Tel Aviv, Israel. ⁹SRON, Netherlands Institute for Space Research, Leiden, The Netherlands. ¹⁰Geneva Observatory, University of Geneva, Sauverny, Switzerland. [✉]e-mail: m.p.stoop@uva.nl

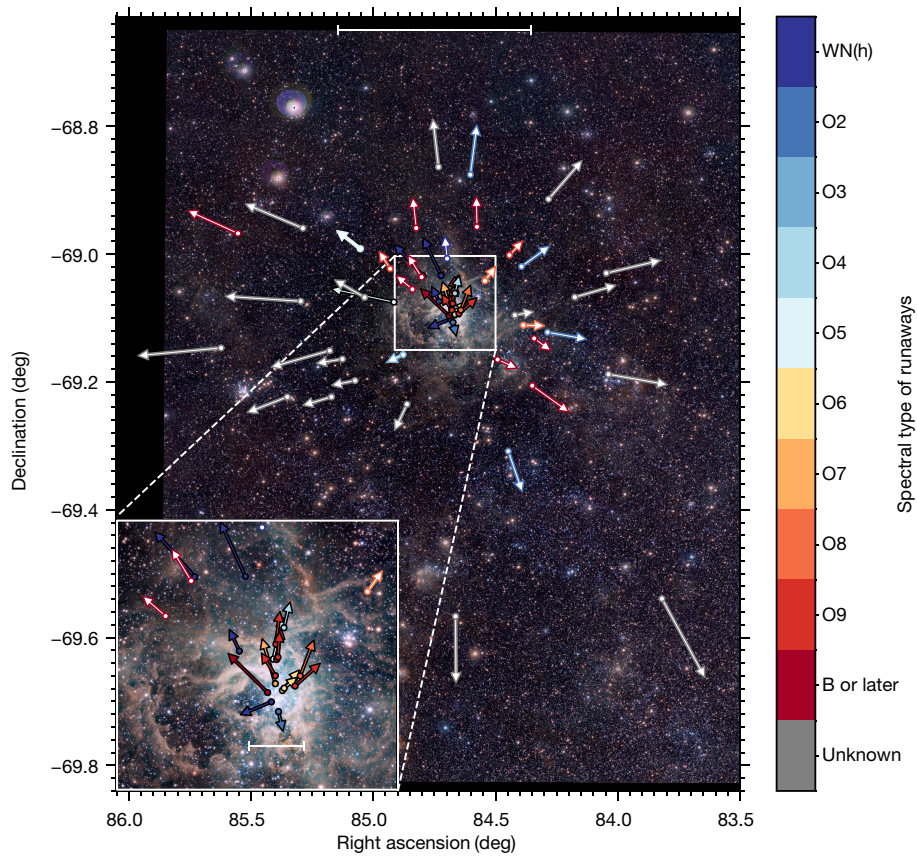


Fig. 1 | On-sky distribution of runaways from R136 in the last 3 Myr. Arrows point in the direction of transverse motion. Their length is proportional to the transverse velocity with respect to R136 (ranging from approximately 28 to 195 km s⁻¹). Black outlined and white filled markers indicate runaways with a kinematic age less or more than 1.0 Myr, respectively. The current position and transverse motion of the runaways are coloured according to spectral type ($n = 55$). The background shows a near-infrared image of the Tarantula nebula (VISTA, credit: ESO/M.-R. Cioni/VISTA Magellanic Cloud survey). Scale bars, 250 pc, 25 pc (inset).

the runaway ejections in the last million years are not associated with this process, a Gaussian fit to the remainder of the sample yielded a mean kinematic age for R136 of $\tau_{\text{kin}} = 1.83^{+0.14}_{-0.10}$ Myr. This provides an independent age estimate of R136, a benchmark star-forming cluster that hosts the most massive stars known^{17–19}.

The evolutionary ages of 21 of the 55 runaways have been estimated (Fig. 4). Out of these 21, 11 have an evolutionary age of over 2.5 Myr,

which is unexpected given the evolutionary age of the stars in R136 (1–2.5 Myr)¹⁷. The more evolved runaways have a median kinematic age of 0.28 Myr and, thus, have been ejected more recently. The evolutionarily younger runaways have a median kinematic age of 1.43 Myr. We performed a K-means clustering analysis, which supported the distinction between the runaways with evolutionary ages of more or less than approximately 2.0–2.5 Myr (Supplementary Information).

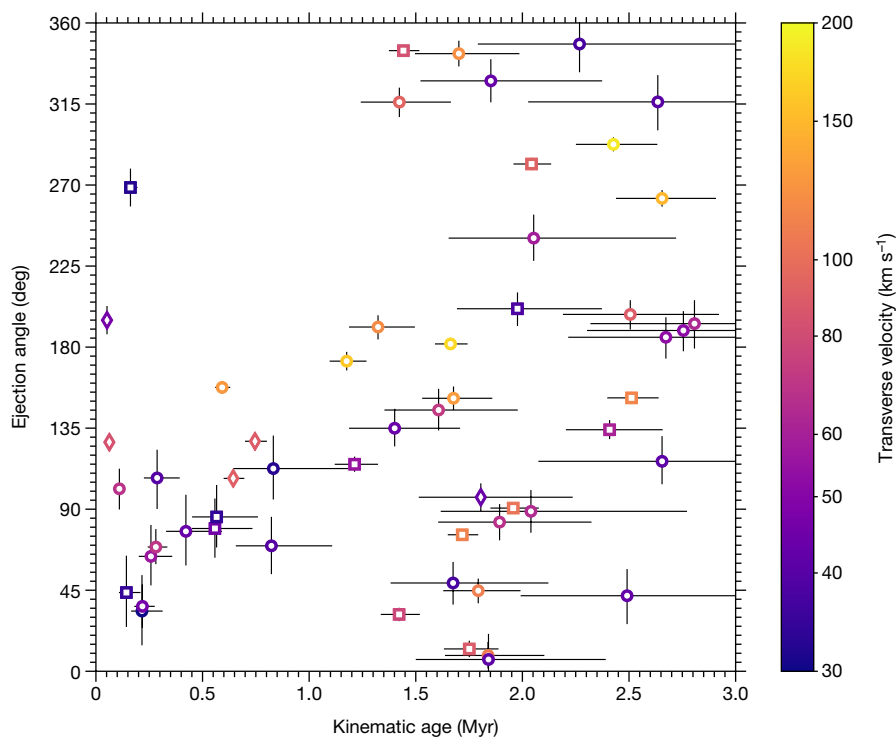


Fig. 2 | Ejection angle and kinematic age distribution of runaways from R136 in the last 3 Myr. The markers are coloured according to their transverse velocity (logarithmic scale). Circles indicate runaways with $15 \text{ mag} < G < 7 \text{ mag}$, squares with $13 \text{ mag} < G < 15 \text{ mag}$ and diamonds the brightest runaways with $11 \text{ mag} < G < 13 \text{ mag}$ ($n = 55$). The uncertainty on the data is expressed as a 1σ confidence interval.

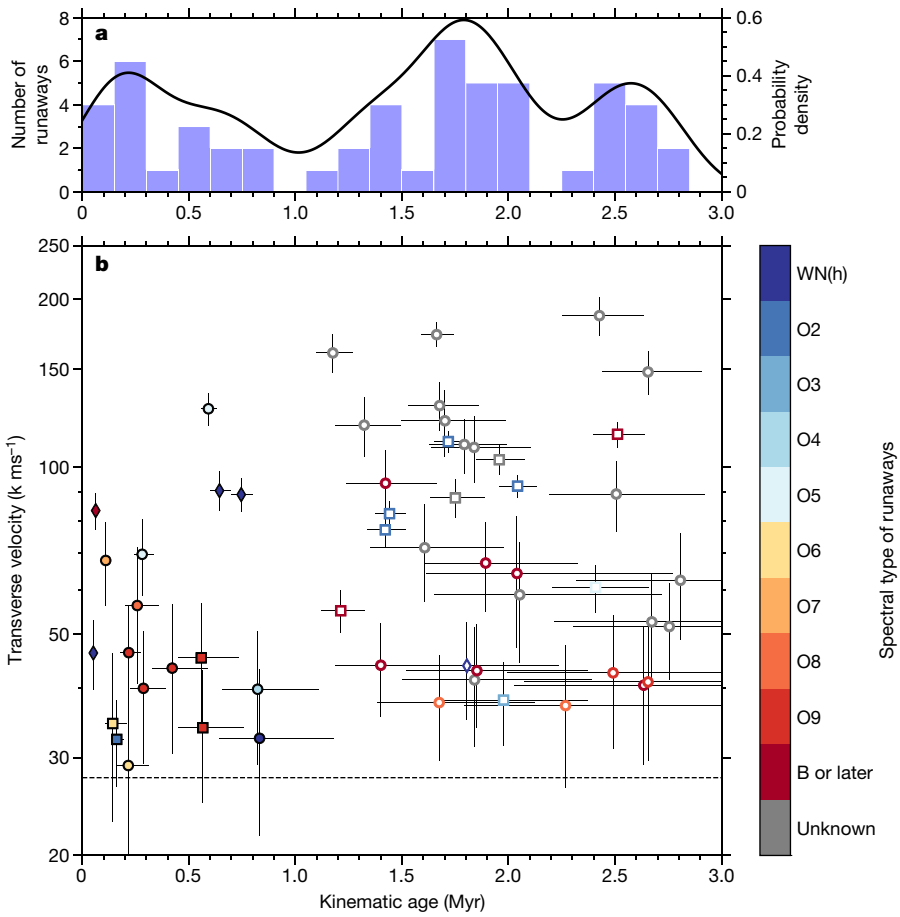


Fig. 3 | Kinematic age and transverse velocity distribution of runaways from R136 in the last 3 Myr. **a**, Histogram of the kinematic ages in blue (left y axis). The Gaussian kernel density estimator (bandwidth of 0.2 Myr) is shown with the black curve (right y axis). **b**, The kinematic age and transverse velocity distribution of runaways coloured according to their spectral type ($n=55$). Circles indicate runaways with $15 \text{ mag} < G < 17 \text{ mag}$, squares with $13 \text{ mag} < G < 15 \text{ mag}$ and diamonds the brightest runaways with $11 \text{ mag} < G < 13 \text{ mag}$. Black outlined and white filled markers indicate runaways ejected with a kinematic age less or greater than 1.0 Myr, respectively. The black dashed line shows the minimum transverse velocity required for a star to be classified as a runaway. The uncertainty on the data is given as a 1σ confidence interval.

The observation of these two different runaway populations suggests that two distinct dynamical ejection mechanisms were at play. The subset of runaways ejected longest ago can be explained by dynamical interactions in the centre of R136 during and shortly after the formation of the cluster. These runaways are consistent with having been ejected isotropically and have an evolutionary age consistent with the age of R136. The runaways launched in a preferred direction are evolutionarily older (3–7 Myr) and were ejected in a distinct episode only about 0.2 Myr ago, approximately 1.5 Myr after the formation of R136. We propose that these runaways were produced by an encounter between R136 and a known nearby cluster that is at present approximately 5.4 pc to the north-east and has an age of 2 to 5 Myr (ref. 20).

We estimated that 33% of the stars born in R136 and more luminous than $\log(L/L_\odot) \geq 6.0$ (and more massive than approximately $60 M_\odot$) have been dynamically ejected from R136. The census of these very luminous stars, both in the R136 core and in the surrounding field, is complete, save for sources heavily obscured by interstellar dust^{21,22}. Counting all non-runaway luminous field stars (Supplementary Information) as originating from the core cluster as well would give a lower limit to the runaway fraction of 23%.

The runaway sample includes WN(h) and O-type stars, of which 30 are spectroscopically confirmed, and four are photometric candidates (Gaia magnitude $G < 16$ mag). N -body simulations of young star clusters with a similar mass as R136 predicted significantly fewer ejections of such stars, typically by a factor of 2 to 6 (refs. 2, 6, 7). A runaway fraction larger than 20% can be obtained only under special physical conditions: a high stellar density, strong primordial mass segregation and a high primordial binary fraction. It is possible that a model that incorporates subcluster merging and the aforementioned starting conditions, but with a larger fraction of primordial wide binaries²³, could reproduce the observed runaway fraction of massive stars.

The more massive runaways initially born in R136 can (partially) explain the shallow slope ($\gamma_{30\text{Dor}} = -1.90^{+0.37}_{-0.26}$) of the stellar initial mass function, relative to the Salpeter slope of $\gamma = -2.35$ (ref. 24), determined in the surrounding 30 Doradus region, which does not include the dense core of R136 (ref. 10). Excluding the five runaways with $M > 60 M_\odot$ also included in the field sample steepens the slope of the mass function to $\gamma_{30\text{Dor}} \approx -2.1$, in marginal agreement with the Salpeter slope²⁴. Inside R136, the estimated slope of the mass function is $\gamma_{\text{R136}} = -2.32 \pm 0.16$ (ref. 17). Correcting the cluster stars for the escaped runaways would make this shallower. We found $\gamma_{\text{R136}} = -1.95 \pm 0.08$ for the stars with masses between 30 and $300 M_\odot$. Thus, star formation in a dense cluster environment such as R136 may produce an initial mass function with a shallower slope at the high-mass end.

The ionizing radiation from a young stellar population such as R136 is dominated by the most massive stars²⁵. The runaways we found contribute 22% to the ionizing budget of the most luminous stars ($\log(L/L_\odot) > 6.0$) in 30 Doradus. Of this budget, 10% is produced by runaways outside the giant molecular cloud that defines 30 Doradus (projected distance to R136 $r_{\text{proj}} > 50$ pc), which provides a lower limit on the H-ionizing photons able to escape the dusty star-forming environment. Luminous early-type stars in faint galaxies at redshifts of approximately 6–15 are thought to constitute the dominant source of ionizing radiation used to explain the cosmological reionization^{26,27}. To reionize the Universe early enough to be consistent with observations, the escape fraction of hydrogen-ionizing photons from these galaxies needs to be $f_{\text{esc}} \gtrsim 5\text{--}20\%$ (refs. 27, 28). Simulations of photon escape from such early galaxies typically yield $f_{\text{esc}} \approx 0.01\text{--}0.1$ (ref. 29), but these simulations do not take into account the effects of runaway stars³⁰. If absorption by dust particles and atomic and molecular gas inside star-forming clouds is the dominant mechanism of Lyman-continuum photon breakdown, the so-far unaccounted for runaway stars may constitute the dominant source of f_{esc} .

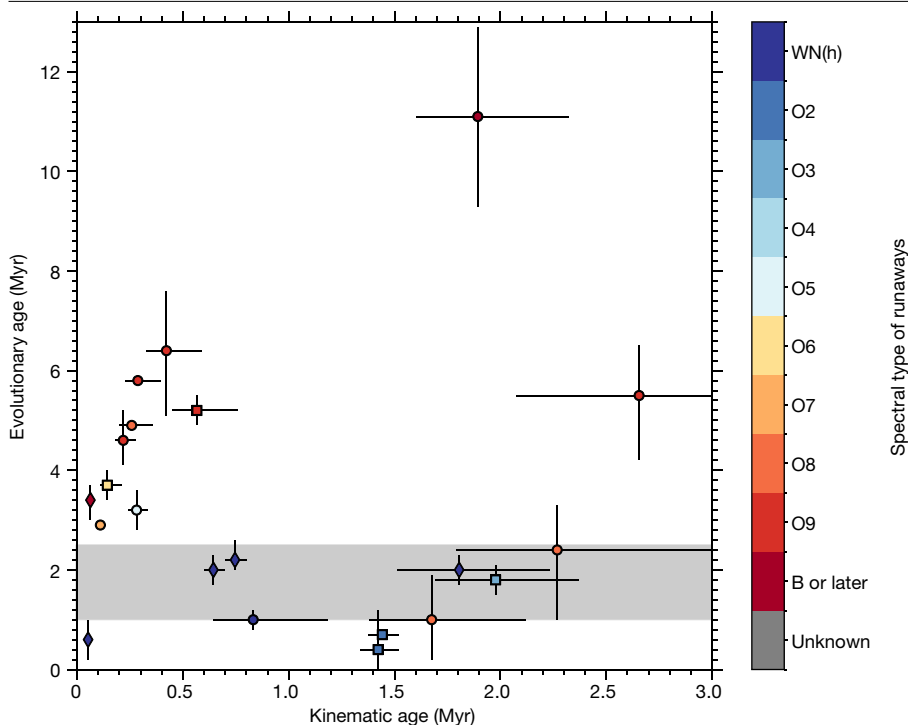


Fig. 4 | Distribution of the runaways' evolutionary age and kinematic age. The markers are coloured according to their spectral type ($n=21$). Circles indicate runaways with $15 \text{ mag} < G < 17 \text{ mag}$, squares with $13 \text{ mag} < G < 15 \text{ mag}$ and diamonds the brightest runaways with $11 \text{ mag} < G < 13 \text{ mag}$. The grey band indicates the age of R136 (1–2.5 Myr)¹⁷. The uncertainty on the data is given as a 1σ confidence interval.

The ionizing radiation and supernovae produced by massive early-type runaways cause efficient heating of the interstellar medium. Hydrodynamical simulations of Milky Way-like spiral galaxies show that the inclusion of a runaway fraction of 14% increases the heating of the interarm medium by an order of magnitude⁸. Runaway stars and their life-ending core-collapse supernovae can also more efficiently (temporarily) expel gas and metals from their host galaxy, which increases the mass and metal loading factor of either a Milky Way-like or dwarf galaxy by a factor 2 to 10 (refs. 8,9), thus significantly affecting the dynamical and chemical evolution of a galaxy.

Online content

Any methods, additional references, Nature Portfolio reporting summaries, source data, extended data, supplementary information, acknowledgements, peer review information; details of author contributions and competing interests; and statements of data and code availability are available at <https://doi.org/10.1038/s41586-024-08013-8>.

- de Wit, W. J., Testi, L., Palla, F. & Zinnecker, H. The origin of massive O-type field stars. II. Field O stars as runaways. *Astron. Astrophys.* **437**, 247–255 (2005).
- Fujii, M. S. & Portegies Zwart, S. The origin of OB runaway stars. *Science* **334**, 1380–1383 (2011).
- Gaia Collaboration. The Gaia mission. *Astron. Astrophys.* **595**, A1 (2016).
- Gaia Collaboration. Gaia Early Data Release 3. Summary of the contents and survey properties. *Astron. Astrophys.* **649**, A1 (2021).
- Gaia Collaboration et al. Gaia Data Release 3. Summary of the content and survey properties. *Astron. Astrophys.* **674**, A1 (2023).
- Banerjee, S., Kroupa, P. & Oh, S. Runaway massive stars from R136: VFTS 682 is very likely a 'slow runaway'. *Astrophys. J.* **746**, 15 (2012).
- Oh, S., Kroupa, P. & Pfleider-Altenburg, J. Dependency of dynamical ejections of O stars on the masses of very young star clusters. *Astrophys. J.* **805**, 92 (2015).
- Andersson, E. P., Agertz, O. & Renaud, F. How runaway stars boost galactic outflows. *Mon. Not. R. Astron. Soc.* **494**, 3328–3341 (2020).
- Steinwandel, U. P., Bryan, G. L., Somerville, R. S., Hayward, C. C. & Burkhardt, B. On the impact of runaway stars on dwarf galaxies with resolved interstellar medium. *Mon. Not. R. Astron. Soc.* **526**, 1408–1427 (2023).
- Schneider, F. R. N. et al. An excess of massive stars in the local 30 Doradus starburst. *Science* **359**, 69–71 (2018).
- Evans, C. J. et al. A massive runaway star from 30 Doradus. *Astrophys. J. Lett.* **715**, 74–79 (2010).
- Lennon, D. J. et al. Gaia DR2 reveals a very massive runaway star ejected from R136. *Astron. Astrophys.* **619**, A78 (2018).

- Sana, H. et al. The VLT-FLAMES Tarantula survey. Observational evidence for two distinct populations of massive runaway stars in 30 Doradus. *Astron. Astrophys.* **668**, L5 (2022).
- Oh, S. & Kroupa, P. Dynamical ejections of massive stars from young star clusters under diverse initial conditions. *Astron. Astrophys.* **590**, A107 (2016).
- Maiz Apellániz, J., Pantaleoni González, M., Barbá, R. H. & Weiler, M. Escape from the Bermuda cluster: orphanization by multiple stellar ejections. *Astron. Astrophys.* **657**, A72 (2022).
- Stoop, M. et al. The early evolution of young massive clusters. II. The kinematic history of NGC 6618/M17. *Astron. Astrophys.* **681**, A21 (2024).
- Brands, S. A. et al. The R136 star cluster dissected with Hubble Space Telescope/STIS. III. The most massive stars and their clumped winds. *Astron. Astrophys.* **663**, A36 (2022).
- Crowther, P. A. et al. The R136 star cluster hosts several stars whose individual masses greatly exceed the accepted $150 M_{\odot}$ stellar mass limit. *Mon. Not. R. Astron. Soc.* **408**, 731–751 (2010).
- Bestenlehner, J. M. et al. The R136 star cluster dissected with Hubble Space Telescope/STIS. II. Physical properties of the most massive stars in R136. *Mon. Not. R. Astron. Soc.* **499**, 1918–1936 (2020).
- Sabbi, E. et al. A double cluster at the core of 30 Doradus. *Astrophys. J. Lett.* **754**, L37 (2012).
- Bestenlehner, J. M. et al. The VLT-FLAMES Tarantula survey. XVII. Physical and wind properties of massive stars at the top of the main sequence. *Astron. Astrophys.* **570**, A38 (2014).
- Crowther, P. A. et al. The R136 star cluster dissected with Hubble Space Telescope/STIS. I. Far-ultraviolet spectroscopic census and the origin of He II $\lambda 1640$ in young star clusters. *Mon. Not. R. Astron. Soc.* **458**, 624–659 (2016).
- Ramírez-Tannus, M. C. et al. A relation between the radial velocity dispersion of young clusters and their age. Evidence for hardening as the formation scenario of massive close binaries. *Astron. Astrophys.* **645**, L10 (2021).
- Salpeter, E. E. The luminosity function and stellar evolution. *Astrophys. J.* **121**, 161 (1955).
- Doran, E. I. et al. The VLT-FLAMES Tarantula survey. XI. A census of the hot luminous stars and their feedback in 30 Doradus. *Astron. Astrophys.* **558**, A134 (2013).
- Barkana, R. & Loeb, A. In the beginning: the first sources of light and the reionization of the Universe. *Phys. Rep.* **349**, 125–238 (2001).
- Wise, J. H. & Cen, R. Ionizing photon escape fractions from high-redshift dwarf galaxies. *Astrophys. J.* **693**, 984–999 (2009).
- Atek, H. et al. Most of the photons that reionized the Universe came from dwarf galaxies. *Nature* **626**, 975–978 (2024).
- Razoumov, A. O. & Sommer-Larsen, J. Modeling Lyman continuum emission from young galaxies. *Astrophys. J.* **668**, 674–681 (2007).
- Connroy, C. & Kratter, K. M. Runaway stars and the escape of ionizing radiation from high-redshift galaxies. *Astrophys. J.* **755**, 123 (2012).

Publisher's note Springer Nature remains neutral with regard to jurisdictional claims in published maps and institutional affiliations.

Springer Nature or its licensor (e.g. a society or other partner) holds exclusive rights to this article under a publishing agreement with the author(s) or other rightsholder(s); author self-archiving of the accepted manuscript version of this article is solely governed by the terms of such publishing agreement and applicable law.

© The Author(s), under exclusive licence to Springer Nature Limited 2024

Methods

Gaia data, filters and corrections

We selected stars in the field in and around 30 Doradus from the Gaia DR3^{3,5}. Taking sources in Gaia DR3 within 1 deg of R136 with $G < 18$ mag resulted in 83,295 sources. This radius is equivalent to approximately 870 pc at the distance of the LMC (49.59 kpc)³¹ and was large enough for us to find runaways with a transverse velocity of up to approximately 290 km s⁻¹ that had been ejected approximately 3 Myr ago. The magnitude cutoff was used to decrease the computation time. Regardless, the other filters described below removed sources with $G \geq 17.5$ mag. A set of corrections and filters was applied to the astrometry. The parallax zero-point offset, estimated from quasars, was used to correct for this bias³². We applied several filters to prevent spurious astrometric solutions from contaminating the runaway sample. First, the astrometry should have a five- or six-parameter astrometric solution. This excluded sources for which no proper motion and parallax could be found. Second, the renormalized unit weight error (ruwe) had to be less than 1.4. A larger ruwe may indicate that the astrometric solution was spurious³³. This may have biased our runaway sample against crowded regions and multiple systems. Third, there should be ten or more visibility periods in the astrometric solution (visibility_periods_used), which is the number of grouped observations used in the astrometric solution. Fewer than ten may be an indication of astrometric or photometric biases⁴. Fourth, we removed sources for which the image parameter determination goodness-of-fit amplitude (ipd_gof_harmonic_amplitude) was larger than 0.15, as this may indicate that the astrometric solution is contaminated by crowding. Similarly, we removed sources for which more than one peak was identified (ipd_frac_multi_peak) in more than 10% of the windows used by Gaia, above which crowding may cause issues in the astrometric solution⁴. Last, sources were excluded for which more than one source identifier was used in the data processing (duplicated_source), which may indicate issues in the astrometric solution. From the 83,295 initially selected sources, we were left with 71,391.

To select sources consistent with being located in the LMC, we removed sources with a parallax ϖ_i larger than 0.15 mas and a parallax uncertainty σ_{ϖ_i} larger than 0.05 mas. At the distance of 49.59 kpc for the LMC ($\varpi_{\text{LMC}} = 0.020$ mas)³¹, the parallax should be less than $\varpi_{\text{LMC}} + 3\sigma_{\varpi_i}$ for each individual source i . This excluded over two thirds of the sources, leaving 21,382 sources. As a result of the parallax constraints, the faintest source has $G \approx 17.4$ mag, implying that the latest or least massive runaway we can detect at the distance of the LMC is a B1–3 V star with a mass of 5–10 M_{\odot} (ref. 34).

Searching for runaways

We searched for massive runaways originating from the centre of R136. To do this, the remaining 21,382 stars in the field in and around 30 Doradus were investigated to identify whether they coincided with the position of R136, taking into account the proper motion of R136 itself. A classical runaway should have a velocity larger than 30 km s⁻¹. The three-dimensional escape velocity of R136 at a distance of 1 pc from the centre, for a cluster mass of $5 \times 10^4 M_{\odot}$, is approximately 21 km s⁻¹ (ref. 22). The radial-velocity dispersion of single massive stars in and around R136 is approximately 3.9 km s⁻¹, which has been corrected for the radial motion of undetected binaries³⁵. For the definition of a runaway, we adopted a transverse velocity difference larger than $5\sigma_{2D} \approx 27.6$ km s⁻¹, where $\sigma_{2D} = \sqrt{2}\sigma_{1D}$. This is close to the runaway threshold velocity in ref. 13, which required a radial velocity deviating from the mean larger than three times the radial-velocity dispersion of all apparently single O stars detected by the VLT-FLAMES Tarantula survey (VFTS) in the 30 Doradus region (approximately 25.8 km s⁻¹). As this is a one-dimensional velocity, there is still a difference by a factor of approximately $\sqrt{2}$. Still undetected multiple systems could exist among the apparent single stars, which could increase the radial-velocity

dispersion. Runaways should not only have a transverse velocity v_T significantly differing from that of R136, but their v_T should also be accurately known. The fractional uncertainty on the transverse velocity v_T/σ_{v_T} should be more than 3, so that v_T is constrained.

We searched for runaways by tracing the stars back using their proper motion. As the R136 cluster also has a proper motion, we subtracted this from each runaway candidate. Runaways were traced back with the equation

$$l_{\text{sep},i}(t) = \left(l_i + \frac{t\mu_{l_i^*}}{3.6 \times 10^6 \cos(b_i)} \right) - \left(l_{\text{R136}} + \frac{t\mu_{l^*,\text{R136}}}{3.6 \times 10^6 \cos(b_{\text{R136}})} \right) \text{deg},$$

$$b_{\text{sep},i}(t) = \left(b_i + \frac{t\mu_{b_i}}{3.6 \times 10^6} \right) - \left(b_{\text{R136}} + \frac{t\mu_{b,\text{R136}}}{3.6 \times 10^6} \right) \text{deg},$$

where t is the time in years. l_{sep} and b_{sep} give the separation of each runaway candidate with respect to the centre of R136. We adopt the Galactic coordinate frame here, with a longitude l , latitude b , proper motion in the longitude direction μ_{l^*} ($\mu_{l^*} = \mu_l \cos(b)$), and proper motion in the latitude direction μ_b . Galactic coordinates have been adopted to minimize the contribution of the $\cos(b)$ factor. The runaway candidates have uncertainties on their proper motion, which is on average 0.045 mas yr⁻¹. This results in an average 1σ uncertainty of approximately 0.02 deg after 1.5 Myr. The radius of R136 is approximately two orders of magnitude smaller (3×10^{-4} deg if adopting a physical radius of 0.3 pc) than the semimajor axis of the 1σ uncertainty ellipse, indicating that we can only trace runaways back to the approximate surroundings of R136 (ref. 36). The position of the runaway candidates should be consistent within 2σ at any time t with that of the centre of R136 following

$$\sqrt{l_{\text{sep},i}^2(t) + b_{\text{sep},i}^2(t)} < \frac{2t}{3.6 \times 10^6} \max(\sigma_{\mu_{l_i^*}}, \sigma_{\mu_{b_i}}) \text{ deg}, \quad (1)$$

where we take the maximum between $\sigma_{\mu_{l^*}}$ and σ_{μ_b} . This indicates that the 2σ uncertainty ellipse should overlap with the centre of R136, and therefore, the position of a runaway is consistent, within 2σ , with an origin in the centre of R136. We traced back the candidate runaways up to 3 Myr ago given the maximum age of R136 (1–2.5 Myr)¹⁷.

Proper motion of R136

To identify runaways, we required prior information on the proper motion of R136. As R136 is a highly crowded region, Gaia resolved no stars with reliable astrometry within several parsecs of the cluster centre. To illustrate this, Extended Data Fig. 1 shows the proper motion of stars with reliable astrometry, as defined above, relative to R136 although these may not necessarily be runaways. Clearly no stars in R136 itself (black circle indicates a radius of 2.0 pc) have reliable astrometry. Information on the proper motion of R136, therefore, must come from the surroundings, which may possibly contain runaways and are known to contain a north-east cluster²⁰. A simple approach is to take the mean or median of the proper motion of these stars in the surroundings and to assume that all proper motions are randomly oriented with respect to R136 and will average out. In this way, ref. 13 estimated $\mu_{\alpha^*,\text{R136}} = 1.700$ mas yr⁻¹ and $\mu_{\delta,\text{R136}} \approx 0.684$ mas yr⁻¹ and ref. 12 estimated $\mu_{\alpha^*,\text{R136}} = 1.739$ mas yr⁻¹ and $\mu_{\delta,\text{R136}} = 0.701$ mas yr⁻¹, where μ_{α^*} is the proper motion in the right ascension direction ($\mu_{\alpha^*} = \mu_{\alpha} \cos(\delta)$), and μ_{δ} is the proper motion in the declination direction.

If the proper motion of the stars surrounding R136 is not random (due to the orbit of the north-east subcluster), this assumption could break down. Instead, we could use the runaways themselves to determine the proper motion of R136. A runaway ejected from the centre of

Article

R136 through dynamical interactions conveys information on where R136 was in the past and, therefore, what the proper motion of R136 is. We kept both $\mu_{l^*,\text{R136}}$ and $\mu_{b,\text{R136}}$ as free parameters in our runaway search and adopted an iterative approach. This method has also been applied to the young massive cluster NGC 6618 in M17 to show that the O-type runaways have all been ejected from within 0.1–0.2 pc from the cluster centre¹⁶.

For an initial estimate of R136's proper motion, we used all runaways satisfying the conditions listed earlier. With these runaways, we redetermined R136's proper motion by minimizing the total $\sqrt{l_{\text{sep,min}}^2(t) + b_{\text{sep,min}}^2(t)}$, normalized to the number of runaways found. As the uncertainties on the proper motion of the runaways differ, we normalized the minimum separation of each runaway with respect to R136 by its uncertainty on the position (the right-hand side of equation (1)). Field-star interlopers could contaminate the runaway sample. We, therefore, used only candidate runaways with a difference between the Gaia Bp and Rp photometric magnitudes ($Bp - Rp < 1.0$ mag, $G < 15$ mag, and a kinematic age $t_{\text{kin}} < 2.25$ Myr to determine R136's proper motion. These stars are consistent with bright early-type stars (see Methods section 'Field stars'), of which most have been classified as O or WN(h)-type stars. The candidate runaways should have $v_T > 25 \text{ km s}^{-1}$, $v_T/\sigma_{v_T} > 2.5$ and $t_{\text{kin}} < 3.0$ Myr, which we calculate from the observed proper motion and uncertainties ignoring correlations. Having redetermined the R136 proper motion, we again search for the runaways. These two steps are iterated until the number of runaways and the R136 proper motion remain unchanged. Six iterations were required, after which 69 candidate runaways were found (with field stars removed).

After obtaining the candidate runaways, we determine v_T and t_{kin} with Markov chain Monte Carlo simulations (see Methods section 'Transverse velocity and kinematic age') and keep the runaways with $v_T > 27.6 \text{ km s}^{-1}$, $v_T/\sigma_{v_T} > 3$ and $t_{\text{kin}} < 3.0$ Myr. This gave a final sample of 55 runaways that were assumed to have been ejected from the centre of R136. We list the astrometric, kinematic and physical parameters of R136 in Extended Data Table 1.

Field stars

The candidate runaways include field-star interlopers. We expected bright early-type stars to be runaways as the faintest candidate runaway has $G \approx 17.4$ mag. However, late-type red giants contaminate the runaway sample. The typical ages of red giants exceed the age of R136 by 2 to 3 orders of magnitude, and they are considered to be interlopers. We distinguished the early-type stars from red giants in colour–colour diagrams such as the ($J - H$) versus ($H - K_s$) diagram in Extended Data Fig. 2 (ref. 37), which used the three photometric filters J , H , and K_s from the Two Micron All-Sky Survey (2MASS). Early-type stars should have $(J - H) \lesssim 0$ mag and $(H - K_s) \lesssim 0$ mag, whereas red giants have $(J - H) \gtrsim 0.5$ mag. Interstellar extinction causes both colours to be reddened, and we show typical reddening lines for an early-type O9 V star and a late-type M0 V star with the black dashed lines (for a total-to-selective extinction $R_v = 3.1$). Even considering interstellar extinction, red giants are in the upper left part of this diagram, whereas early-type stars should be on the O-type reddening line. We have excluded stars consistent with the late-type part of this diagram indicated with the grey region. The reddened runaway VFTS 682, with spectral type WN5h, is shown with the blue star (with extinction $A_v = 4.45 \pm 0.45$)³⁸, which overlaps the O9 V reddening line.

2MASS JHK_s photometry is not available for nearly half of the stars with $G > 15$ mag. We show the Gaia colour–magnitude diagram in Extended Data Fig. 3. The previously determined early-type stars are shown with blue circles and the late-type stars with red squares. Candidate runaways with unavailable or poor 2MASS photometry are shown with open symbols. Almost all stars with $G_{\text{Bp}} - G_{\text{Rp}} \gtrsim 1.0$ mag were determined to be late-type stars from the near-infrared colour–colour diagram, except for two. One of these is VFTS 682, whereas we classified

the second star (purple open square) as a red giant and the 33 stars with $G_{\text{Bp}} - G_{\text{Rp}} < 1.0$ mag as early-type stars (golden open circles). A reasonable assumption is that early-type stars should have $G_{\text{Bp}} - G_{\text{Rp}} < 1.0$ and only VFTS 682 is an exception. VFTS 682 is a well-studied WN(h) star³⁸ and had already been identified as a potential runaway from R136 (ref. 39). We excluded the red supergiant MH18, which is shown in the top right of Extended Data Fig. 3 ($v_T \approx 60 \text{ km s}^{-1}$).

Transverse velocity and kinematic age

We determined the transverse velocity and the kinematic age of each runaway with Markov chain Monte Carlo simulations. For each runaway, the three observables are $(\varpi_i, \mu_{l^*,i}, \mu_{b,i})$ with a corresponding 3 by 3 covariance matrix. The three random variables are the distance d_i , transverse velocity $v_{T,i}$ and ejection angle ϕ_i . The distance prior $\theta(d_i)$ is a Gaussian distance distribution with a mean of 49.59 kpc and a standard deviation of 0.011 kpc (ref. 31). We adopted a uniform prior on the transverse velocity $\theta(v_{T,i})$ between 0 and 250 km s^{-1} and ejection angle $\theta(\phi_i)$ between 0 and 2π rad. From this, we calculated the three variables:

$$\begin{aligned}\varpi_i &= 1/d_i \text{ mas,} \\ \mu_{l^*,i} &= \frac{v_{T,i} \sin(\phi_i)}{4.74047 d_i} \text{ mas yr}^{-1}, \\ \mu_{b,i} &= \frac{v_{T,i} \cos(\phi_i)}{4.74047 d_i} \text{ mas yr}^{-1}.\end{aligned}$$

For each runaway, we drew four chains each containing 100,000 iterations to determine the posterior samples. With the inference data, the kinematic age was determined as the time that minimizes the separation between the runaway and R136. Assuming that the runaways were ejected from R136, we used the iterations for the kinematic age for which the minimum separation between the runaway and R136 was less than 0.005 deg (approximately 5 pc at the distance of the LMC). The v_T and t_{kin} of a runaway were given by the 50th percentiles, with a positive and negative 1σ uncertainty determined by the 13.6th and 86.4th percentiles, respectively.

Luminous stars in 30 Doradus

We list all the luminous stars in 30 Doradus with $\log(L/L_\odot) > 6.0$ in Extended Data Table 2. This list includes stars inside the core of R136, in the surrounding halo around R136 and in the 30 Doradus nebula^{10,17,21}. We included MCPS 084.44781-69.30846 and SK-68 137, both of which are O2-3 stars consistent with $\log(L/L_\odot) > 6.0$. They are outside the 30 Doradus region and no stellar parameters have been determined for them. For these two stars and VFTS 512, we took their stellar parameters as the average of the luminous stars in R136 with a similar spectral type. The stellar parameters were obtained from the literature^{40–52}.

We determined the runaway fraction (RF) of the stars using $\log(L/L_\odot)$ as

$$RF = \frac{R}{CL + R} \times 100\% = 33\%,$$

where R is the number of runaway stars ($n = 12$) and CL is the number of cluster stars ($n = 25$). We defined stars to be part of R136 if they have a projected distance with respect to R136 $r_{\text{proj}} < 10$ pc, except for Melnick 34 and VFTS 512, which we determined to be runaways. There are field stars in 30 Doradus that are neither runaways nor cluster stars ($n = 15$). These field stars may still have originated from R136 but have not reached the escape velocity, and they may be on wide elliptical orbits. Several field stars have $ruwe > 1.4$, making it impossible to draw conclusions on their origin. We also calculated the runaway fraction as

$$RF = \frac{R}{CL + FLD + R} \times 100\% = 23\%,$$

where FLD is the number of field stars. This is a lower limit for the runaway fraction, as was found for Galactic O stars⁵³. Extended Data Fig. 4 shows the location of the runaway, cluster and field stars in and outside the 30 Doradus nebula. If we have missed runaways near R136, either because (systemic) radial velocities have not been determined or because the Gaia astrometry is not accurate, then the minimum runaway fraction may be higher. A radial-velocity search for O-type runaways in the 30 Doradus region yielded at least one candidate with an evolutionary age less than 3.0 Myr and a mass of approximately more than $60 M_{\odot}$ (ref. 13).

Data availability

The datasets generated during or analysed during the current study are available at Zenodo (<https://doi.org/10.5281/zenodo.10058762>)⁵⁴.

Code availability

The software and code described in this paper and used to produce the findings are available at Zenodo (<https://doi.org/10.5281/zenodo.10058762>)⁵⁴.

31. Pietrzyński, G. et al. A distance to the Large Magellanic Cloud that is precise to one per cent. *Nature* **567**, 200–203 (2019).
32. Lindegren, L. et al. Gaia Early Data Release 3. Parallax bias versus magnitude, colour, and position. *Astron. Astrophys.* **649**, A4 (2021).
33. Lindegren, L. Re-normalising the astrometric chi-square in Gaia DR2. Report No. GAIA-C3-TN-LU-LL-124 (Gaia Collaboration, Semantic Scholar, 2018).
34. Pecaut, M. J. & Mamajek, E. E. Intrinsic colors, temperatures, and bolometric corrections of pre-main-sequence stars. *Astrophys. J. Suppl. Ser.* **208**, 9 (2013).
35. Héault-Brunet, V. et al. The VLT-FLAMES Tarantula survey. VII. A low velocity dispersion for the young massive cluster R136. *Astron. Astrophys.* **546**, A73 (2012).
36. Portegies Zwart, S. F., McMillan, S. L. W. & Gieles, M. Young massive star clusters. *Annu. Rev. Astron. Astrophys.* **48**, 431–493 (2010).
37. Skrutskie, M. F. et al. The Two Micron All Sky Survey (2MASS). *Astron. J.* **131**, 1163–1183 (2006).
38. Bestenlehner, J. M. et al. The VLT-FLAMES Tarantula Survey. III. A very massive star in apparent isolation from the massive cluster R136. *Astron. Astrophys.* **530**, L14 (2011).
39. Renzo, M. et al. Space astrometry of the very massive $\sim 150 M_{\odot}$ candidate runaway star VFTS682. *Mon. Not. R. Astron. Soc.* **482**, 102–106 (2019).
40. Brands, S. A. et al. Extinction towards the cluster R136 in the Large Magellanic Cloud. An extinction law from the near-infrared to the ultraviolet. *Astron. Astrophys.* **673**, A132 (2023).
41. Tehrani, K. A. et al. Weighing Melnick 34: the most massive binary system known. *Mon. Not. R. Astron. Soc.* **484**, 2692–2710 (2019).
42. Schnurr, O., Moffat, A. F. J., St-Louis, N., Morrell, N. I. & Guerrero, M. A. A spectroscopic survey of WNL stars in the Large Magellanic Cloud: general properties and binary status. *Mon. Not. R. Astron. Soc.* **389**, 806–828 (2008).
43. Shenar, T. et al. The Wolf-Rayet binaries of the nitrogen sequence in the Large Magellanic Cloud. Spectroscopy, orbital analysis, formation, and evolution. *Astron. Astrophys.* **627**, A151 (2019).
44. Castro, N. et al. Mapping the core of the Tarantula nebula with VLT-MUSE. I. Spectral and nebular content around R136. *Astron. Astrophys.* **614**, A147 (2018).
45. Sana, H. et al. The VLT-FLAMES Tarantula survey. VIII. Multiplicity properties of the O-type star population. *Astron. Astrophys.* **550**, A107 (2013).
46. Mahy, L. et al. The Tarantula massive binary monitoring. III. Atmosphere analysis of double-lined spectroscopic systems. *Astron. Astrophys.* **634**, A118 (2020).
47. Shenar, T. et al. The Tarantula massive binary monitoring. V. R 144: a wind-eclipsing binary with a total mass $\gtrsim 140 M_{\odot}$. *Astron. Astrophys.* **650**, A147 (2021).
48. Sabin-Sanjulián, C. et al. The VLT-FLAMES Tarantula survey. XXVI. Properties of the O-dwarf population in 30 Doradus. *Astron. Astrophys.* **601**, A79 (2017).
49. McEvoy, C. M. et al. The VLT-FLAMES Tarantula Survey. XIX. B-type supergiants: atmospheric parameters and nitrogen abundances to investigate the role of binarity and the width of the main sequence. *Astron. Astrophys.* **575**, A70 (2015).
50. Evans, C. J., van Loon, J. T., Hainich, R. & Bailey, M. 2dF-AAOmega spectroscopy of massive stars in the Magellanic Clouds. The north-eastern region of the Large Magellanic Cloud. *Astron. Astrophys.* **584**, A5 (2015).
51. Walborn, N. R., Lennon, D. J., Haser, S. M., Kudritzki, R.-P. & Voels, S. A. The physics of massive OB stars in different parent galaxies. I. Ultraviolet and optical spectral morphology in the Magellanic Clouds. *Publ. Astron. Soc. Pac.* **107**, 104 (1995).
52. Walborn, N. R. et al. A CNO dichotomy among O2 giant spectra in the Magellanic Clouds. *Astrophys. J.* **608**, 1028–1038 (2004).
53. Carretero-Castrillo, M., Ribó, M. & Paredes, J. M. Galactic runaway O and Be stars found using Gaia DR3. *Astron. Astrophys.* **679**, A109 (2023).
54. Stoop, M. et al. Reproduction package for the paper ‘Two waves of massive stars running away from the young cluster R136’. Zenodo <https://doi.org/10.5281/zenodo.10058762> (2024).

Acknowledgements We thank F. Backs, O. Ould-Boukattine, J. Hessels, D. Linssen and M. Snelders for their help and discussions. M.S. acknowledges support from NOVA. The research leading to these results has received funding from the European Research Council under the European Union’s Horizon 2020 research and innovation programme (grant agreement no. 772225: MULTIPLES). This work has made use of data from the European Space Agency’s mission Gaia (<https://www.cosmos.esa.int/gaia>), which were processed by the Gaia Data Processing and Analysis Consortium (<https://www.cosmos.esa.int/web/gaia/dpac/consortium>). Funding for the consortium was provided by national institutions, in particular the institutions participating in the Gaia multilateral agreement. This publication makes use of data products from 2MASS, which is a joint project of the University of Massachusetts and the Infrared Processing and Analysis Center/California Institute of Technology and is funded by NASA and the National Science Foundation.

Author contributions M.S. led the runaway search and data analysis, produced all the figures and tables, and was the main contributor to the text. A.d.K. and L.K. contributed to the scientific interpretation, context and text. S.B. contributed to the results, implications and text. S.P.Z. and H.S. contributed to the scientific interpretation, implications and context. F.S. contributed to the statistical interpretation. All other authors contributed towards the discussion and provided feedback on the text.

Competing interests The authors declare no competing interests.

Additional information

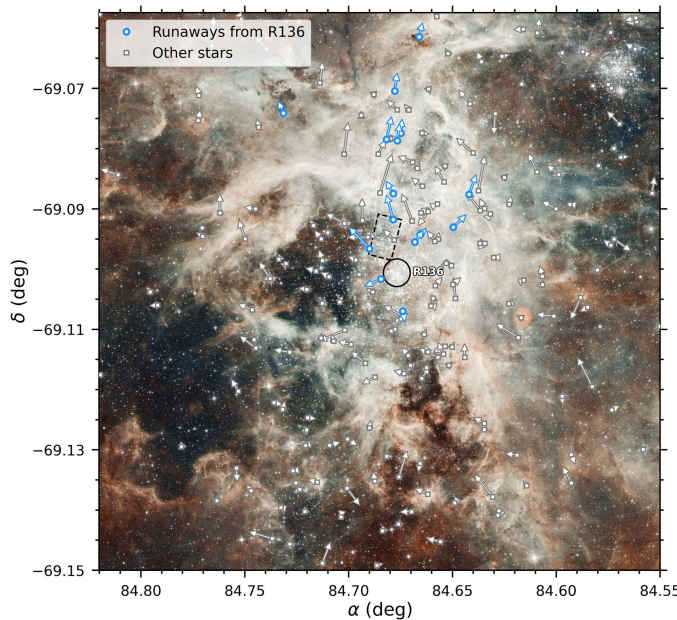
Supplementary information The online version contains supplementary material available at <https://doi.org/10.1038/s41586-024-08013-8>.

Correspondence and requests for materials should be addressed to Mitchel Stoop.

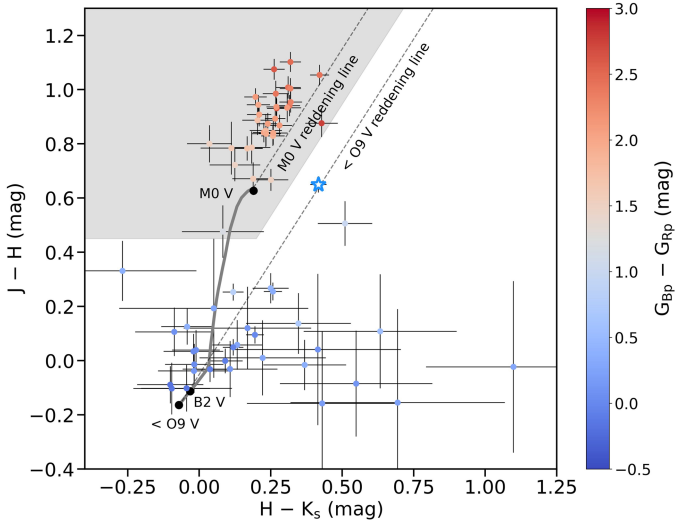
Peer review information Nature thanks Sara Berlanas and Elena Sabbi for their contribution to the peer review of this work. Peer reviewer reports are available.

Reprints and permissions information is available at <http://www.nature.com/reprints>.

Article

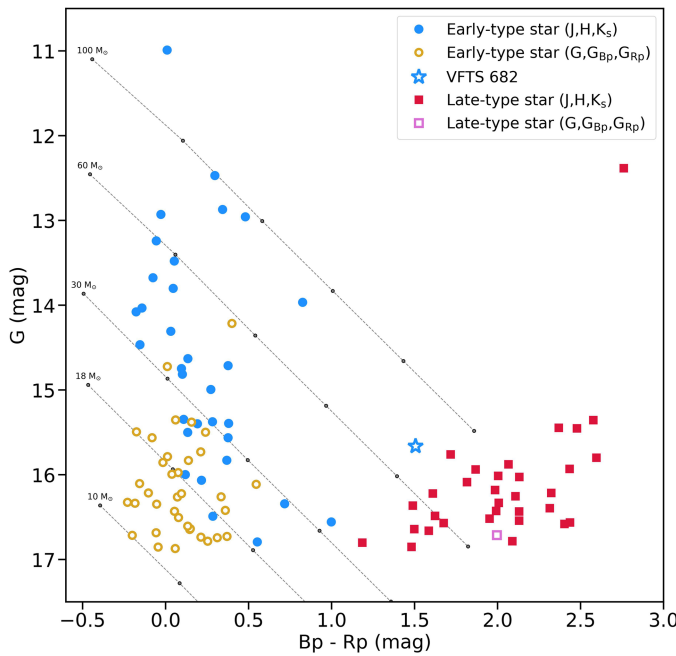


Extended Data Fig. 1 | Proper motion of stars relative to R136 in the field in and around R136 with reliable astrometry. The blue stars represent the runaways coming from R136 found in this work, while the grey stars do not originate in R136. The stars with reliable astrometry are defined in Section 1. The proper motion of R136 found in Section 1 has been subtracted and is $\mu_{\alpha^*,\text{R136}} = 1.654 \text{ mas yr}^{-1}$ and $\mu_{\delta,\text{R136}} = 0.573 \text{ mas yr}^{-1}$. The black circle is centred on R136 and has a radius of 2.0 pc. The dashed black rectangle depicts the region used to derive the colour-magnitude-diagram of the north-east cluster in²⁰. The background image is taken by the *Hubble Space Telescope* (*HST*) and European Southern Observatory (ESO) 2.2m telescope (image credit: NASA, ESA and D. Lennon et al., 2012).

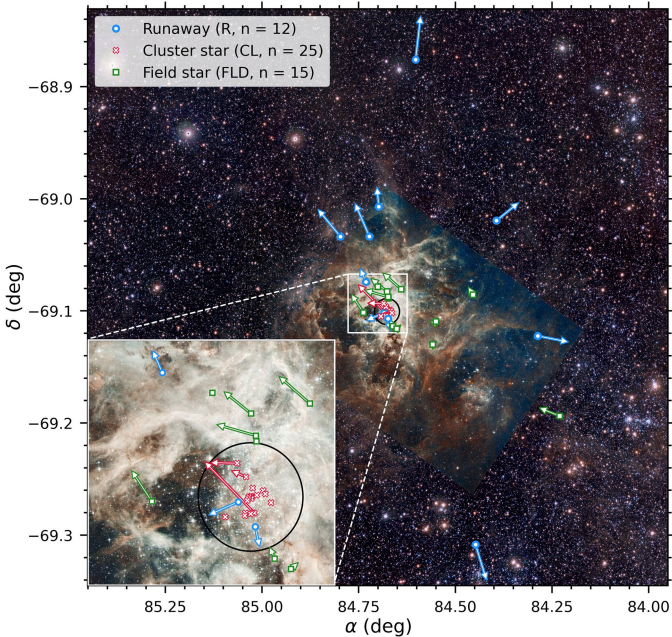


Extended Data Fig. 2 | Near-infrared (2MASS) colour-colour diagram of the runaway candidates. They are coloured according to their *Gaia* colour $G_{\text{bp}} - G_{\text{rp}}$. The location of an O-type (<O9 V), B2 V, and M0 V star on the zero-age-main-sequence in this diagram are indicated with the black circles³⁴. The location of main-sequence stars with spectral types between O9 V and M0 V are represented by the grey curve. The reddening lines for the O9 and MO dwarf star are given with the black dashed lines. The reddened WN5h star VFTS 682 is shown with the open blue star. Stars in the grey shaded region in the upper left corner are excluded from the final runaway sample as they are consistent with late-type stars. The uncertainty on the data is given as a 1σ confidence interval.

Article



Extended Data Fig. 3 | Gaia colour magnitude diagram (CMD) of the runaway candidates. Stars with blue circles and red squares were included and excluded, respectively, based on Extended Data Fig. 2. Parsec reddening lines are shown for a 10, 16, 30, 60, and 100 M_⊙ star with the grey dots denoting A_v equal to 0.0 to 5.0 mag in steps of 1.0 mag ($R_V = 3.1$) for an age = 1.8 Myr. The relatively reddened WNSh star VFTS 682 is shown with the open blue star. The open yellow circles are included in the final runaway sample on the basis of their relatively blue colour. The open purple square is excluded based on its relatively red colour. The star located in the upper right is the red supergiant MH18 that could be a massive runaway star.



Extended Data Fig. 4 | On-sky distribution of the most luminous stars ($\log[L/L_\odot] > 6.0$) in R136 and 30 Doradus. Arrows depict the transverse motion direction and the length of the arrows are proportional to the transverse velocity with respect to R136. Blue circles depict runaways coming from R136, red crosses denote stars which are classified as member of R136 ($r_{\text{proj}} < 10 \text{ pc}$), and green squares indicate stars which are neither runaways originating from R136 nor member of R136. The foreground image is a composite image from the *Hubble Space Telescope (HST)* and European Southern Observatory (ESO) 2.2m telescope (image credit: NASA, ESA D. Lennon et al., 2012). The background shows a near-infrared image of the Tarantula Nebula produced by the ESO Visible and Infrared Survey Telescope for Astronomy (VISTA, credit: ESO/M.-R. Cioni/VISTA Magellanic Cloud survey).

Article

Extended Data Table 1 | Astrometric, kinematic, and physical parameters of R136

Equatorial		
Right Ascension*	α	84.67664 deg
Declination*	δ	-69.10084 deg
Proper motion†	μ_α^*	1.654 mas yr ⁻¹
Proper motion†	μ_δ	0.573 mas yr ⁻¹
μ_α^* dispersion	σ_α	-
μ_δ dispersion	σ_δ	-
Galactic		
Galactic longitude*	l	279.46505 deg
Galactic latitude*	b	-31.67190 deg
Proper motion†	μ_l^*	-0.757 mas yr ⁻¹
Proper motion†	μ_b	1.578 mas yr ⁻¹
μ_l^* dispersion	σ_l	-
μ_b dispersion	σ_b	-
Radial		
Parallax [31]	ϖ	0.0202 mas
Distance [31]	d	$49.59 \pm 0.09 (\pm 0.54)$ kpc
Radial velocity [13]	v_R	268.2 ± 8.6 km s ⁻¹
v_R dispersion [35]	σ_R	4-5 km s ⁻¹
Physical properties		
Mass [22]	M_{cl}	$\sim 5 \cdot 10^4 M_\odot$
Radius [40]	r_{cl}	~ 0.1 pc
Age (runaways)	-	$1.83^{+0.15}_{-0.10}$ Myr
Age (literature) [17]	-	1.0-2.5 Myr
Visual extinction [41]	A_V	1.70 ± 0.45 mag
Number of O stars‡	-	$\sim 4 \cdot 10^2$

*R136a1 is assumed to be the centre of R136. †Estimated using the runaways, see main text.

‡Extrapolating the IMF slope (-1.95) between 18–300 M_\odot assuming $M_{\text{cl}} = 5 \times 10^4 M_\odot$.

Extended Data Table 2 | All stars in 30 Doradus with $\log(L/L_\odot) > 6.0$

Identifier	Spectral type	$r_{\text{sep,proj}}$ pc	$\log(L/L_\odot)$	v_R km s^{-1}	$\log(Q_0)$ s^{-1}	Ref.
R 136a1	W N5h	0.0*	6.86	-	50.71	[17, 19, 22]
R 136a2	W N5h	0.02	6.71	-	50.59	[17, 19, 22]
R 136a5	O 2 I(n)f*	0.07	6.32	-	50.13	[17, 19, 22]
R 136a7	O 3 III(f*)	0.09	6.36	-	50.21	[17, 19, 22]
R 136a3	W N5h	0.12	6.7	-	50.56	[17, 19, 22]
R 136a8	-	0.12	6.17	-	49.98	[17, 19, 22]
R 136a4	O 3 V((f*))(n)	0.14	6.28	-	50.10	[17, 19, 22]
R 136a6	O 2 I(n)f*p	0.19	6.24	-	50.10	[17, 19, 22]
H 36	O 2 If*	0.38	6.27	-	50.10	[17, 19, 22]
H 46	O 2-3 III(f*)	0.43	6.1	-	49.96	[17, 19, 22]
R 136b	O 4 If	0.52	6.35	-	50.00	[17, 19, 22]
R 136c	W N5h	0.90	6.58	-	50.32	[21]
VFTS 1014	O 3 V + mid/late O	1.22	6.22	-	50.00	[21]
Melnick 42	O 2 If*	1.70	6.56	-	50.37	[21]
Melnick 34 A	W N5h	2.52	6.43	287 ± 5	50.39 [†]	[25, 42]
Melnick 34 B	W N5h	2.52	6.43	287 ± 5	50.39 [†]	[25, 42]
VFTS 1001	W N6h	2.70	6.20	-	49.96	[21, 43, 44]
VFTS 482 AB	O 2.5 If*/W N6	2.89	6.40	226 ± 13	50.14	[21, 45]
VFTS 1021	O 4 If+	2.96	6.34	-	50.02	[21]
VFTS 1017	O 2 If*/W N5	3.04	6.21	-	50.05	[21]
VFTS 1022	O 3.5 If*/W N7	3.11	6.48	-	50.22	[21]
VFTS 545	O 2 If*/W N5	3.12	6.30	-	50.11	[21]
VFTS 1028	O 3 III(f*) or O 4-5 V	3.62	6.09	280 ± 6	49.91	[21, 43, 45]
VFTS 542	O 2 If*/W N5 + B0 V	3.78	6.16	269 ± 8	49.94	[21, 43]
VFTS 468	O 2 V((f*)) + OB	4.06	6.00	-	49.79	[21]
VFTS 512 AB	O 2 V-III(f*) + ?	5.57	6.04	-	49.86	[21, 46]
VFTS 599	O 3 III(f*)	6.06	6.01	265.0 ± 1.3	49.77	[10, 21, 46]
VFTS 562	O 4 V	6.74	6.05	278 ± 8	49.79	[21, 46]
VFTS 506 AB	O N2 V((n))((f*)) + ?	10.33	6.24	-	50.05	[21, 46]
VFTS 509 AB	W N5(h) + O 4 V	11.35	6.09	220 ± 10	50.17	[21, 44]
VFTS 457	O 3.5 If*/W N7	12.27	6.20	-	49.89	[21]
VFTS 427	W N8(h)	15.38	6.13	-	49.90	[21]
VFTS 527 A	O 6.5 I	15.38	6.20	262.4 ± 0.1	49.78 [†]	[25, 47]
VFTS 527 B	O 7 I	15.38	6.20	262.4 ± 0.1	49.78 [†]	[25, 47]
VFTS 695 A	W N6h	18.85	6.35	270 ± 5	49.74 [†]	[25, 44]
VFTS 695 B	O 3.5 If/W N7	18.85	6.35	270 ± 5	49.74 [†]	[25, 44]
VFTS 621	O 2 V((f*))z	20.54	6.14	-	49.97	[21]
VFTS 402	W N5(h) + W N7(h):	20.62	6.07	274 ± 9	49.69	[21, 44]
VFTS 682	W N5h	28.45	6.51	300 ± 10	50.35	[21]
VFTS 259 A	O 6 Iaf	39.82	6.1	-	49.71	[21]
VFTS 267 A	O 3 III-I(n)f*	44.5	6.01	-	49.79	[21]
R 144 A	W N5/6h	59.67	6.44	210 ± 20	49.95 [†]	[25, 48]
R 144 B	W N6/7h	59.67	6.44	210 ± 20	49.95 [†]	[25, 48]
VFTS 758	W N5h	68.75	6.36	-	50.17	[21]
R 130 A	WC 4	69.88	6.01	332 ± 7	49.60 [†]	[25, 44]
R 130 B	B1Ia	69.88	6.07	332 ± 7	49.60 [†]	[25, 44]
VFTS 617	W N5ha	83.36	6.29	-	50.14	[21]
VFTS 72	O 2 V-III(n)((f*))	112.21	5.96-6.06	273.6 ± 2.2	49.75-49.93	[21, 49]
VFTS 16	O 2 III-If*	121.67	6.12	189.4 ± 1.3	50.08	[21]
VFTS 3	B1 Ia+	159.48	6.03	-	47.62 [†]	[50]
M CPS 084.44781-69.30846	O 2-3 V-III(f*)	193.12	5.5-6.1 [§]	277.9 ± 2.9	49.3-49.9 [§]	[51]
SK -68 137	O 2-3.5 III(f*)	195.85	6.19	273	50.07 [‡]	[52, 53]

The uncertainty on the data is expressed as a 1 σ confidence interval. *R136a1 is assumed to be the centre of R136. Each component in the binary is assumed to contribute half of the total ionising photons. [†]Estimated in this work, see main text. [§]Range is given by the lower and upper values of stars with similar spectral types in R136.